

## Deep Core Convection and Dynamo in Newly-born Neutron Star

YOUHEI MASADA,<sup>1</sup> TOMOYA TAKIWAKI,<sup>2</sup> AND KEI KOTAKE<sup>3</sup><sup>1</sup>*Department of Science Education, Aichi University of Education, Kariya 448-8542, Japan*<sup>2</sup>*Division of Science, National Astronomical Observatory of Japan, Tokyo 181-8588, Japan*<sup>3</sup>*Faculty of Science, Department of Applied Physics & Research Institute of Stellar Explosive Phenomena, Fukuoka University, Fukuoka 814-0180, Japan*

(Received January 23, 2020)

Submitted to ApJL

## ABSTRACT

We report results from a convection dynamo simulation of proto-neutron star (PNS), with a nuclear equation of state (EOS) and the initial hydrodynamic profile taken from a neutrino radiation-hydrodynamics simulation of a massive stellar core-collapse. A moderately-rotating PNS with the spin period of 170 ms in the lepton-driven convection stage is focused. We find that large-scale flow and thermodynamic fields with north-south asymmetry develop in the turbulent flow, as a consequence of the convection in the central part of the PNS, which we call as a “deep core convection”. Intriguingly, even with such a moderate rotation, large-scale,  $10^{15}$  G, magnetic field with dipole symmetry is spontaneously built up in the PNS. The turbulent electro-motive force arising from rotationally-constrained core convection is shown to play a key role in the large-scale dynamo. The large-scale structures organized in the PNS may impact the explosion dynamics of supernovae and subsequent evolution to the neutron stars.

**Keywords:** convection — dynamo — magnetohydrodynamics (MHD) — stars: magnetic field — stars: neutron

## 1. INTRODUCTION

Neutron stars (NSs) have the most extreme magnetic field in the universe, typically trillion, up to quadrillion times more powerful than Earth’s. Although, we know, they are formed as an aftermath of massive stellar core-collapse, the origin of the magnetic fields is still an outstanding issue in astrophysics. Mainly, two possible origins have been proposed: fossil field and dynamo field hypotheses (e.g., Spruit 2008; Ferrario et al. 2015). While the former regards it as an inheritance from NS’s main sequence progenitor (e.g., Ruderman 1972), the later presumes that it would be generated by some dynamo processes in the newly-born NSs, also known as proto-neutron stars (PNSs) (e.g., Ruderman & Sutherland 1973; Thompson & Duncan 1993, hereafter TD93).

One important physical process, which should be examined further in either scenarios, is the role of PNS convection. Even if the strong fossil field exists before the collapse, it should be subjected to vigorous convective motions after the formation of the PNS (e.g., Epstein 1979; Burrows & Latimer 1988; Keil et al. 1996). It is not fully discussed whether the structure and coherency of the fossil magnetic field are re-

tained in such a tumultuous situation. At least, independent from the spin rate of the PNS, the turbulent convection would strongly disturb, locally amplify, and transport the fossil field (Nordlund et al. 1994), unless the field strength is stronger than the equipartitioned one. The characteristics of the fossil field acquired before core-collapse thus seems likely to be lost during the evolution of the PNS. On the flip side, in the dynamo hypothesis, the convective motion would play a vital role in generating the large-scale magnetic field in the PNS.

The convective dynamo in the PNS is discussed in TD93 theoretically under the modern scenario of the core-collapse supernova. In the context of the  $\alpha$ - $\Omega$  dynamo (e.g., Parker 1955), they argue that a large-scale magnetic field with  $\mathcal{O}(10^{15})$  G, is generated only when the spin period of the PNS ( $\equiv P_{\text{rot}}$ ) is shorter than  $\mathcal{O}(10)$  ms. This constraint comes from the prerequisite for operating the large-scale convective dynamo (e.g., Moffatt 1978; Krause & Raedler 1980): *the Rossby number should be smaller than unity*, that is  $Ro \equiv v/(2\Omega l) \lesssim 1$ , where the spin rate  $\Omega$ , the typical velocity and length-scale  $v$  and  $l$  with their chosen values  $v \simeq \mathcal{O}(10^3)$  km/s and  $l \simeq \mathcal{O}(0.1)$  km, corresponding to the convection velocity and scale-height expected in the outer region of the PNS. In the ordinary PNS with  $P_{\text{rot}} \gtrsim \mathcal{O}(10)$  ms (Ott et al. 2006), the large-scale magnetic field does not grow and the small-scale “patchy” magnetic structures would pre-

vail. This is the standard, but still rough, framework they constructed for the PNS dynamo.

The aim of our study is to give shape to the theory of the PNS convection and dynamo in a more quantitative, self-consistent manner. Different from the earlier numerical studies based on the mean-field dynamics with given profiles of turbulent electro-motive force and differential rotation (e.g., Bonanno et al. 2003, 2006), we solve the magnetohydrodynamics (MHD) of PNS convection. As the first step, we construct a “PNS in a box” simulation model with a nuclear EOS and a realistic initial condition just after the core-bounce of stellar collapse, and then perform a MHD convection simulation with focusing on a moderately-rotating PNS.

## 2. NUMERICAL SETUP

We study the convective dynamo in the PNS with “star in a box” model (Dobler et al. 2006). To cover the whole sphere from the center to pseudo-surface, the PNS is described as a spherical subregion of radius  $R_{\text{PNS}}$  of a cubic box of size  $L_{\text{box}}^3$  and is solved in the Cartesian grids  $(x, y, z)$ . The spherical coordinates  $(r, \theta, \phi)$  are used for analysis. The baryon in the box is governed by fully-compressible non-relativistic MHD equations. The lepton transport is additionally solved under the diffusion approximation. Basic equations are written, in a rotating reference frame with an angular velocity  $\Omega_0$ , as

$$\frac{D\rho}{Dt} + \rho \nabla \cdot \mathbf{v} = 0, \quad (1)$$

$$\begin{aligned} \frac{D\mathbf{v}}{Dt} = & -2\Omega_0 \mathbf{e}_z \times \mathbf{v} - \frac{1}{\rho} \nabla P + \frac{1}{4\pi\rho} (\nabla \times \mathbf{B}) \times \mathbf{B} \\ & + \frac{2}{\rho} \nabla \cdot (\rho \nu \mathbf{S}) + \mathbf{g} + \mathbf{f}_{\text{damp}}, \end{aligned} \quad (2)$$

$$\begin{aligned} \frac{D\epsilon}{Dt} = & -\frac{P \nabla \cdot \mathbf{v}}{\rho} + 2\nu \mathbf{S}^2 \\ & + \frac{\eta (\nabla \times \mathbf{B})^2}{4\pi\rho} + \frac{\gamma \nabla \cdot (\kappa \nabla \epsilon)}{\rho} + \dot{\epsilon}_{\text{damp}}, \end{aligned} \quad (3)$$

$$\frac{\partial \mathbf{B}}{\partial t} = \nabla \times (\mathbf{v} \times \mathbf{B} - \eta \nabla \times \mathbf{B}), \quad (4)$$

$$\frac{DY_e}{Dt} = \nabla \cdot (\xi \nabla Y_e) + \dot{Y}_{e,\text{source}}, \quad (5)$$

with the strain rate tensor  $S_{ij} \equiv (\partial_j v_i + \partial_i v_j - 2\delta_{ij} \partial_i v_i / 3) / 2$ , where  $\epsilon$  is the specific internal energy,  $Y_e$  is the lepton fraction and the other symbols have their usual meanings. The viscous, magnetic, heat, and lepton diffusivities are given by  $\nu, \eta, \kappa$  and  $\xi$ , respectively. Damping terms  $\mathbf{f}_{\text{damp}}$  and  $\dot{\epsilon}_{\text{damp}}$ , which keep  $\mathbf{v}$  and  $\epsilon$  outside the PNS close to the initial profiles to avoid boundary artifacts, are given by

$$\mathbf{f}_{\text{damp}} = -\frac{\mathbf{v}}{\tau_d} f_{\text{ext}}, \quad \dot{\epsilon}_{\text{damp}} = \frac{\epsilon_{\text{ini}} - \epsilon}{\tau_d} f_{\text{ext}}, \quad (6)$$

with  $f_{\text{ext}} = (1 + \tanh[(r - R_{\text{PNS}})/w_t])/2$ , where  $\epsilon_{\text{ini}}$  is the initial profile of  $\epsilon$ ,  $\tau_d$  is the damping time and  $w_t$  is the width of the transition layer between the PNS and the

“buffer” damping region. For maintaining the lepton gradient, the source term is added to the lepton transport equation

$$\dot{Y}_{e,\text{source}} = \frac{Y_{e,\text{ini}} - Y_e}{\tau_s} f_{\text{int}} \quad (7)$$

with  $f_{\text{int}} = (1 - \tanh[(r - R_{\text{PNS}})/w_t])/2$ , where  $Y_{e,\text{ini}}$  is the initial profile of  $Y_e$  and  $\tau_s$  is the forcing time. This is a simple model for the replenishment of the lepton via the energy conversion from the gravity to the neutrino radiation inside the PNS during its cooling time. To close the system, we employ the EOS by Lattimer & Swesty (1991) with a compressibility modulus of  $K = 220$  MeV.

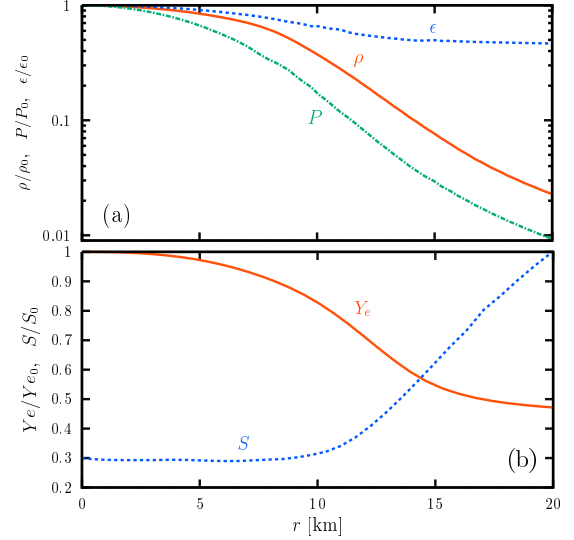


**Figure 1.** Radial distributions of (a)  $\rho$ ,  $P$  and  $\epsilon$ , and (b)  $Y_e$  and  $S$  of the initial model. Normalizations are  $\rho_0 = 2.5 \times 10^{14}$  g/cm<sup>3</sup>,  $P_0 = 5.86 \times 10^{33}$  dyn/cm<sup>2</sup>,  $\epsilon_0 = 5.85 \times 10^{19}$  erg/g,  $Y_{e0} = 0.35$ , and  $S_0 = 3.96 k_B$ .

We set an initial equilibrium model based on a post-bounce core from a hydrodynamic simulation of core-collapse of  $15 M_\odot$  progenitor, see Masada et al. (2015) for details. About 100 ms after the core bounce, the shock wave has reached  $\sim 200$  km, and the PNS is settled into a quasi-hydrostatic state. The hydrodynamic variables within  $0 \leq r \leq 20$  km ( $\equiv L_{\text{box}}/2$ ) are extracted, and then the PNS is reconstructed with a 2nd-order interpolation method in the calculation domain ranging  $-L_{\text{box}}/2 \leq x, y, z \leq L_{\text{box}}/2$ .

Shown in Figure 1 are radial distributions of (a)  $\rho$ ,  $P$  and  $\epsilon$ , and (b)  $Y_e$  and  $S$  (entropy) of the initial model. The negative lepton gradient which lies in the inner part of the PNS powers the lepton-driven convection (e.g., Epstein 1979; Keil et al. 1996). In contrast, the outer region where  $r \gtrsim 15$  km is stable to the convective instability based on the Ledoux criterion (e.g., Ledoux 1947; Kippenhahn, & Weigert 1990). Since the outer convectively stable layer has less impact on the hydrodynamics of the PNS during the evolution time of interest, the pseudo-surface of the PNS is chosen here as  $R_{\text{PNS}} = 17.5$  km. We connect the PNS to the outer buffer region through the transition layer with  $w_t = 0.05 R_{\text{PNS}}$ .

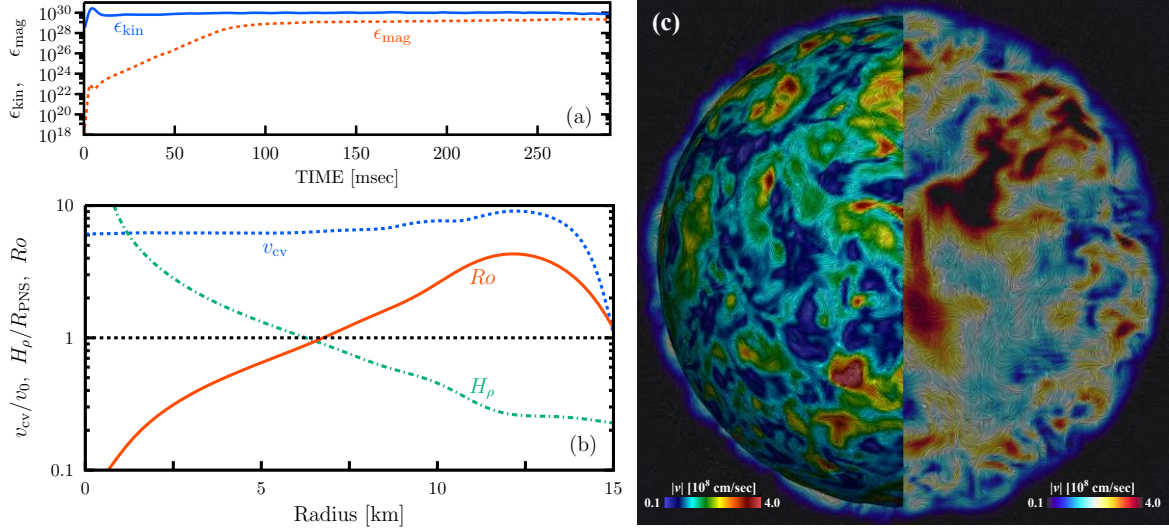


**Figure 2.** (a) Temporal-evolution of volume-averaged kinetic (blue-solid) and magnetic (red-dashed) energies. (b) Radial profiles of time and spherical averages of  $(v_r^2)^{1/2}$  ( $\equiv v_{\text{cv}}$ , blue-dashed),  $H_\rho$  (green dash-dotted) and  $Ro$  (red solid). Time average is taken over  $220 \leq t \leq 240$  ms. Normalization unit is  $v_0 = 1.5 \times 10^7$  cm/s. (c) LIC visualizations of  $|\mathbf{v}|$  at  $r = 15$  km (left hemisphere) and meridional cutting plane (right hemisphere) when  $t = 230$  ms. Red (blue) tone denotes higher (lower) convection velocity.

The forcing time for the lepton is assumed to be constant inside the PNS and an order of magnitude shorter than the typical convective turn-over time, that is  $\tau_s = 0.1\tau_{\text{cv}}$ , where  $\tau_{\text{cv}} \equiv l_{\text{sh}}/v_{\text{cv}}$  with the typical convection velocity  $v_{\text{cv}} = 10^8$  cm/s and the typical scale-height  $l_{\text{sh}} = 10^5$  cm. With this value, we can keep the profile of  $Y_e$  close to, but slightly deviate from, the initial state. To reduce the boundary artifacts as much as possible, a short damping time of  $\tau_d = 0.1\tau_s$  is adopted. We choose, as a first step, uniform diffusivities of  $\nu = \eta = \kappa = \xi = 10^{11}$  cm<sup>2</sup>/s inside the PNS. While  $\nu$ ,  $\kappa$  and  $\xi$  assumed here are within the expectations in the PNS,  $\eta$  is far from realistic ( $\eta_{\text{PNS}} \sim 10^{-5}$  cm<sup>2</sup>/s) (e.g., Masada et al. 2007) because of a numerical limitation as is so often the case with the planetary and stellar dynamo simulations (e.g., Jones 2011; Brun & Browning 2017).

The governing equations are solved by the second-order Godunov-type finite-difference scheme which employs an approximate MHD Riemann solver (see Sano et al. 1999; Masada et al. 2012, 2015, for details). The box is resolved by  $N^3 = 256^3$  grid points. In the following, we present the result of the convective dynamo simulation of a moderately-rotating PNS with  $\Omega_0 = 12\pi$  s<sup>-1</sup>. After a random small “seed” magnetic field with the amplitude  $|\delta B| < 10^9$  G is introduced into the PNS, the calculation is started by adding a small perturbation to the initial pressure distribution.

### 3. RESULTS

The rough sketch of the simulation results is summarized in Figure 2. Time evolution of the volume-averaged kinetic and magnetic energies is shown in panel (a). When the simulation proceeds, the lepton-driven convection begins to grow and then both the kinetic and magnetic energies are amplified in the PNS. While the convective energy saturates within  $\sim 50$  ms, the magnetic energy gradually increases

and reaches a quasi-steady state after  $t \sim 200$  ms. Since the PNS is fully convective, there exists, even in the central region, vigorous flows with  $\mathcal{O}(10^8)$  cm/s as found in Figure 2(b) where the radial profiles of the mean convection velocity, the scale-height and the local Rossby number defined by  $Ro = v_{\text{cv}}/(2\Omega H_\rho)$  are also shown. The structure of the convection on the PNS surface or the meridional cutting plane is shown in Figure 2(c). The size of convective cells becomes larger with the depth because of the larger scale-height in the deeper region, achieving the low Rossby number state, i.e.,  $Ro < 1$ , in the PNS core (see also, Figures 2(b)). As will be discussed later, such a rotationally-constrained core convection is the key for the spontaneous formation of large-scale magnetic fields in our PNS model.

As a corollary of the core convection, large-scale flow and thermodynamic fields are organized in the PNS. We focus on these quantities before explaining the dynamo activity. Meridional distributions of (a)  $\langle v_\theta \rangle$ , (b)  $\delta\epsilon \equiv \langle \epsilon - \bar{\epsilon} \rangle$  and (c)  $\Omega \equiv \langle v_\phi \rangle / r \sin \theta$  are shown in Figure 3, where over-bar denotes the time and spherical ( $\theta, \phi$ ) average and angular brackets denote the time- and azimuthal average. The over-plotted arrows in panel (a) are meridional velocity vectors.

The mean meridional flow shows a single-cell counter-clockwise profile with circulating between northern and southern hemispheres with the velocity of  $\mathcal{O}(10^8)$  cm/s. This structure should be due to a dipole dominance of the convective flow which is shown, in the linear study (§ 59 of Chandrasekhar (1961)), to be a natural topological result of the full-spherical convection domain: northern and southern hemispheres are dominated respectively by faster (and cool) downflow and slower (and warm) upflow (see fig. 2(c)), yielding the formation of the large-scale coherent circulation in-between them.

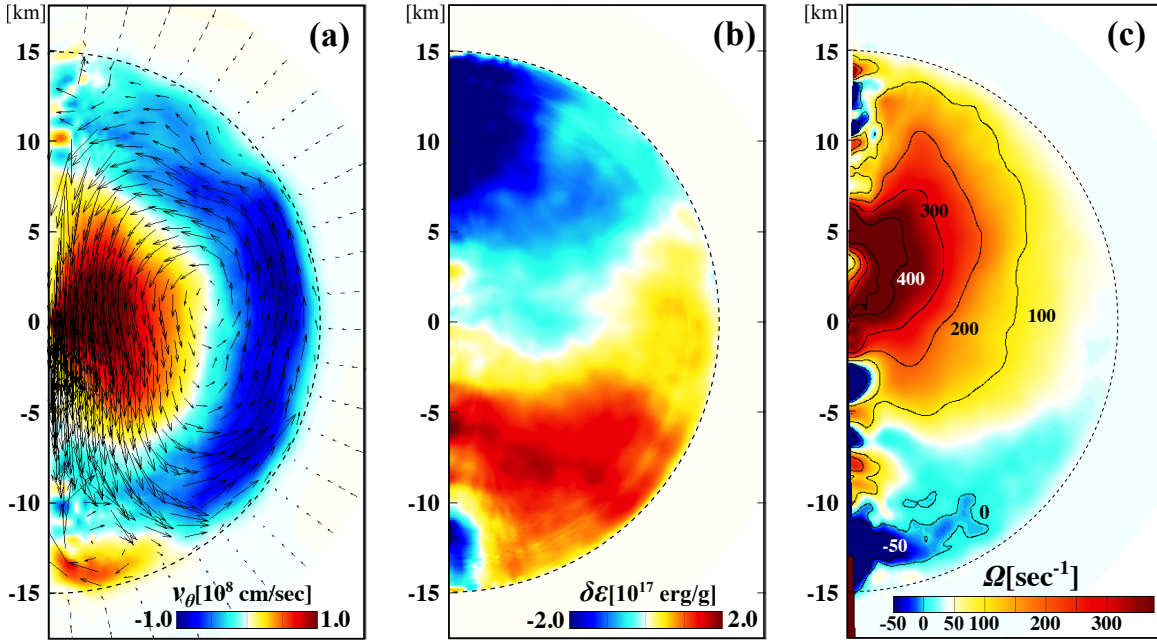


**Figure 3.** Meridional distributions of (a)  $\langle v_\theta \rangle$ , (b)  $\delta\epsilon$  and (c)  $\Omega$ . In panel (a), the streamlines are overplotted with an arrow length proportional to the flow velocity. In panel (c), the region rotating with the reference frame  $\Omega_0$  is shown by white color. The iso-rotation contours of  $\Omega = -50, 0, 100, 200, 300$ , and  $400 \text{ s}^{-1}$  are also overplotted.

The dipole-dominance of the convective motion, i.e., the “cool” downflow in the north and the “warm” upflow in the south, results in the antisymmetric profile of  $\delta\epsilon$  with respect to the equator. The difference of  $\delta\epsilon$  between hemispheres is averagely  $4 \times 10^{17} \text{ erg/g}$  which provides  $10^{50} - 10^{51} \text{ erg}$  in the total volume of the PNS, possibly aiding to arise an asymmetry in supernovae even in the collapses of moderately-rotating progenitor stars. Furthermore, if  $\mathcal{O}(1) \%$  of the energy difference can be converted to the kinetic energy of the bulk motion of the NS, it may be able to account for the NS’s proper motion with  $\mathcal{O}(10^2) \text{ km/s}$  (e.g., [Hobbs et al. 2005](#)).

The profile of  $\Omega$  should be determined to retain a quasi-steady convective state: the production of vorticity by the baroclinic term ( $\propto \partial\epsilon/\partial\theta$ ) should be balanced mainly with the production of relative vorticity by the stretching ( $\propto \partial\Omega/\partial z$ ), that is, the thermal wind balance

$$\frac{\partial\omega}{\partial t} = r \sin\theta \frac{\partial\Omega^2}{\partial z} - \frac{g}{\gamma\bar{\epsilon}} \frac{\partial\epsilon}{\partial\theta} \dots = 0, \quad (8)$$

should be maintained (e.g., [Pedlosky 1982](#); [Masada 2011](#)), where  $\omega$  is the vorticity. This is consistent with what we observe in the simulation, i.e., differential rotation with a north-south asymmetry (fig.2 (c)), which progrades in the north and retrogrades in the southern hemisphere of the PNS. The overall mean properties of the hydrodynamics seen in our PNS model are analogous to those in [Brun & Palacios \(2009\)](#) though their simulated object is the red giant.

Primarily, the turbulent convective motion produces small-scale magnetic fields. Figure 4 shows, in the Mollweide projection, the distribution of the radial component of the magnetic field on the spherical surfaces at different depths. It is found that the turbulent component of the magnetic field

becomes predominant inside the PNS. It should be amplified via small-scale convective dynamo (e.g., [Cattaneo 1999](#); [Schekochihin et al. 2004](#)) and finally reaches to  $\mathcal{O}(10^{16}) \text{ G}$ , which contains the energy of about 40 % of the convective kinetic energy at the saturated stage (see fig.2(a)).

In such a haystack of turbulent magnetic components, surprisingly, the large-scale magnetic structure is spontaneously organized in our PNS model. Figure 5 shows the meridional distributions of large-scale magnetic components, (a)  $\langle B_r \rangle$ , (b)  $\langle B_\theta \rangle$  and (c)  $\langle B_\phi \rangle$ . The global structure of the mean magnetic component exhibits a dipole dominance. It can be found that the large-scale poloidal component, rooted deep in the central part of the PNS, shows a strong dipole symmetry, while it is less coherent in the outer part of the sphere. The strength of it maximally reaches  $10^{15} \text{ G}$ , which is compatible with that expected in the strongly-magnetized NSs, so-called “magnetars”. In contrast to the poloidal component, a large-scale toroidal magnetic component is built up mainly in the outer part of the PNS. It is roughly antisymmetric with respect to the equator and has an average strength of  $\mathcal{O}(10^{14}) \text{ G}$ . As well as the mean flow field, the large-scale magnetic structure is not transient but is maintained for a relatively long time, indicating that it should be the self-organized structure as a natural outcome of the symmetry breaking forced by the NS’s spin. The mechanism for the large-scale dynamo in our system is discussed in § 4.

#### 4. DISCUSSION

It is well known that the rotating convection system spontaneously generates a mean kinetic helicity with a north-south antisymmetry, i.e., in the case of the eastward rotation like our PNS model, bulk positive helicity in north and negative



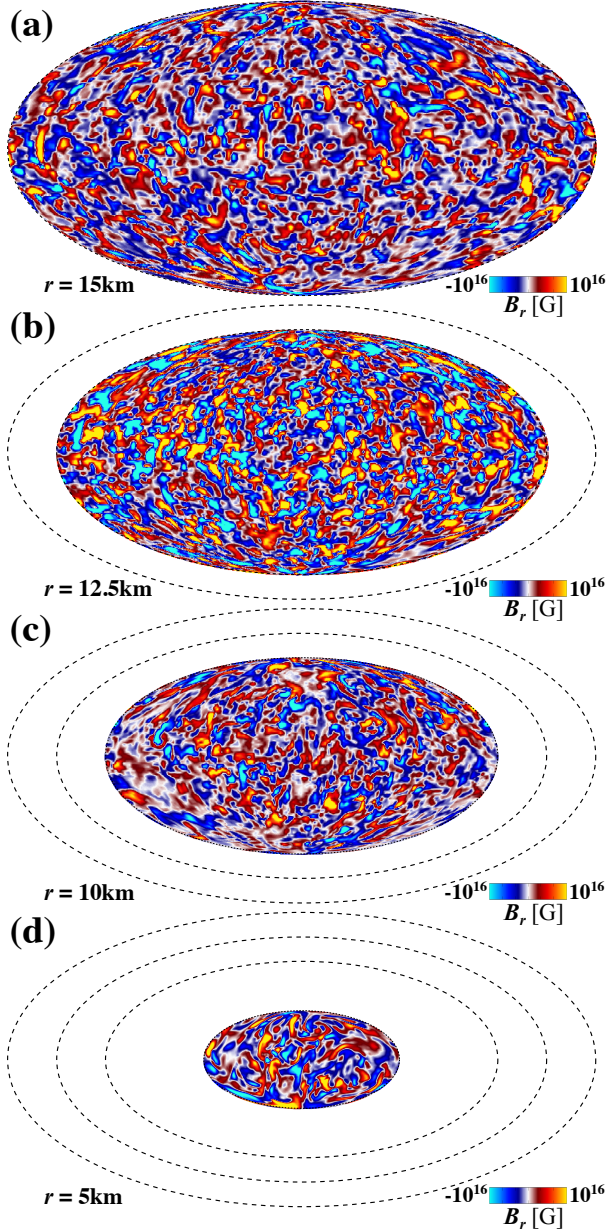


**Figure 4.** Distributions of the radial component of the magnetic field on spherical surfaces at sampled radii  $r = 15\text{km}$ ,  $12.5\text{km}$ ,  $10\text{km}$ , and  $5\text{km}$  when  $t = 230\text{ ms}$  in the Mollweide projection.

in south, because of the Coriolis force acting on the convection flow (e.g., Miesch 2005). From preceding studies on stellar and solar dynamos (e.g., Charbonneau 2014; Brun & Browning 2017, for reviews), we expect that the mean kinetic helicity and its accompanying turbulent electro-motive fore (EMF) would be the origin of the large-scale magnetic component even in our PNS system (e.g., Racine et al. 2011; Masada & Sano 2014).

Although it is difficult to evaluate quantitatively the role of the turbulent EMF in the complicated PNS dynamo system, we can appraise it at least qualitatively based on the mean-

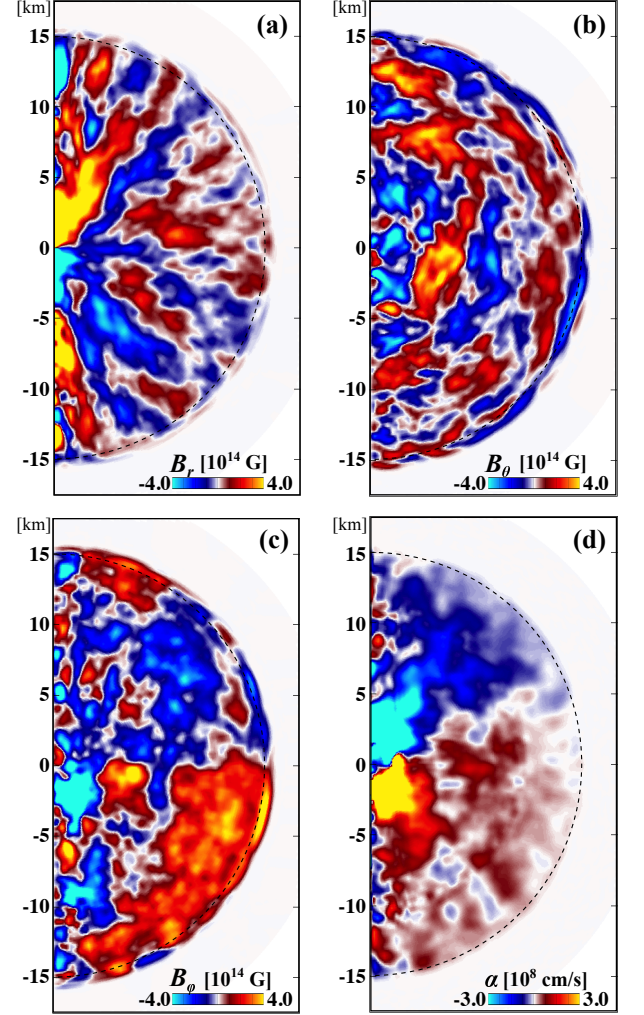


**Figure 5.** Meridional distributions of large-scale magnetic components, (a)  $\langle B_r \rangle$ , (b)  $\langle B_\theta \rangle$ , (c)  $\langle B_\phi \rangle$ , and (d) the turbulent  $\alpha$ . The time average is taken over the duration  $220 \leq t \leq 240\text{ ms}$ .

field dynamo (MFD) theory. Under the first-order smoothing approximation (e.g., Brandenburg & Subramanian 2005; Masada & Sano 2014), the kinetic helicity would be closely linked to the turbulent  $\alpha$ -effect, which is a key ingredient for generating the large-scale magnetic field in the MFD framework (e.g., Moffatt 1978; Krause & Raedler 1980), as

$$\alpha \equiv -\tau_{\text{cor}} \langle \mathbf{v}' \cdot \boldsymbol{\omega}' \rangle / 3, \quad (9)$$

where  $\mathbf{v}' \equiv \mathbf{v} - \langle \mathbf{v} \rangle$  is the turbulent velocity,  $\tau_{\text{cor}}$  is the correlation time and  $\boldsymbol{\omega}' \equiv \nabla \times \mathbf{v}'$  is the turbulent vorticity. With an estimation  $\tau_{\text{cor}} = H_\rho / \langle v_r^2 \rangle^{1/2}$ , we can evaluate the turbulent  $\alpha$ -effect from the simulation data directly.

To examine the connection between the large-scale magnetic structure and the turbulent  $\alpha$ -effect, we show the meridional distribution of the turbulent  $\alpha$  which is derived directly from the simulation data in Figure 5(d). It can be found that there exists a remarkable overlap between the region with the large-scale magnetic structure, especially poloidal component, and that with the strong  $\alpha$ -effect. This suggests that

the turbulent EMF plays a major role in the PNS dynamo, especially in the core region. In contrast, since the region where the toroidal component is well-organized is a bit apart from there, the  $\Omega$ -effect, i.e., wrapping process of the magnetic field by differential rotation, is most likely dominant over the  $\alpha$ -effect.

Although the convective dynamo is believed conventionally to work only in rapidly rotating PNSs (e.g., TD93), we find a clear dynamo activity even in the moderately-rotating PNS with  $P_{\text{rot}} = 170$  ms. The dynamo activity is sustained by the rotationally-constrained convection, i.e.,  $Ro < 1$  state, which is realized in the deeper part of the PNS (fig.2(a)).

As demonstrated in the 2D hydrodynamic simulation of the deleptonization of the PNS by Keil et al. (1996), the convection zone in the PNS enlarges to the deeper part with the progress of the neutrino cooling, finally encompassing the whole star within  $\sim 1$  s after bounce, and can continue for at least as long as the deleptonization takes place. Since most of the existing studies for the PNS dynamo supposes the early evolutionary stage at which only the outer part of the PNS is convective, the scale-height, thus the size of the convective cell, is relatively small there, resulting in the high Rossby number dynamo in the case with the slow or moderate rotation (e.g., TD93). On the other hand, the PNS, which we studied here with supposing the later evolutionary stage, is in the core convection state and has a larger convective cell in the deeper part. In such a situation, the Coriolis force dominates over the inertia force around the PNS core, and thus the large-scale magnetic component should be efficiently amplified there by the turbulent  $\alpha$ -effect against the turbulent diffusion. We note that the importance of the deep core convection for the large-scale dynamo has already been pointed out in the study for the origin of the magnetic field in the fully-convective M-type dwarfs (Yadav et al. 2016).

## 5. SUMMARY

We found from our numerical study that large-scale flow, thermodynamic and magnetic fields are spontaneously organized inside the PNS as the natural consequence of the deep core convection : the single-cell meridional flow with circulating between northern and southern hemispheres, the differential rotation with north-south asymmetry, the north-south antisymmetric profile of  $\delta\epsilon$ , and the large-scale magnetic component with the dipole dominance. We also showed that the possible ingredient for the large-scale dynamo is the rotationally-constrained core convection, which is not fully considered in the standard PNS dynamo theory.

Recently, fully-nonlinear numerical studies on the PNS convection and dynamo rapidly advance with the increase of the computational power. Nagakura et al. (2019) shows, in their systematic hydrodynamic study of the CCSNs, that the PNS convection commonly occurs independent from the progenitor mass. Furthermore, Raynaud et al. (2020) confirms, for the first time, that the large-scale convective dynamo successfully occurs in the rapidly-rotating PNS. To build up the concrete view on the role of the PNS convection, the parametric studies, such as dependencies on the spin rate, diffusivities, and structure of the PNS, should be our future work.

## ACKNOWLEDGMENTS

This work has been supported by MEXT/JSPS KAKENHI Grant Numbers JP17H01130, JP17K14306, JP18H01212, JP18K03700, JP17H06357, JP17H06364, JP18H04444; the Central Research Institute of Stellar Explosive Phenomena (REISEP) at Fukuoka University and the associated projects (Nos. 171042,177103) and JICFuS as a priority issue to be tackled by using Post ‘K’ Computer. Numerical computations were carried out on Cray XC50 at Center for Computational Astrophysics, National Astronomical Observatory of Japan.

## REFERENCES

- Bonanno, A., Rezzolla, L., & Urpin, V. 2003, *A&A*, 410, L33  
 Bonanno, A., Urpin, V., & Belvedere, G. 2006, *A&A*, 451, 1049  
 Brun, A. S., & Palacios, A. 2009, *ApJ*, 702, 1078  
 Brun, A. S., García, R. A., Houdek, G., et al. 2015, *SSRv*, 196, 303  
 Brun, A. S., & Browning, M. K. 2017, *Living Reviews in Solar Physics*, 14, 4  
 Brandenburg, A., & Subramanian, K. 2005, *PhR*, 417, 1  
 Burrows, A., & Lattimer, J. M. 1988, *PhR*, 163, 51  
 Cattaneo, F. 1999, *ApJL*, 515, L39  
 Chandrasekhar, S. 1961, *Hydrodynamic and Hydromagnetic Stability* (Oxford: Clarendon)  
 Charbonneau, P. 2014, *ARA&A*, 52, 251  
 Dobler, W., Stix, M., & Brandenburg, A. 2006, *ApJ*, 638, 336  
 Epstein, R. I. 1979, *MNRAS*, 188, 305  
 Ferrario, L., Melatos, A., & Zrake, J. 2015, *SSRv*, 191, 77  
 Hobbs, G., Lorimer, D. R., Lyne, A. G., et al. 2005, *MNRAS*, 360, 974  
 Jones, C. A. 2011, *Annual Review of Fluid Mechanics*, 43, 583  
 Keil, W., Janka, H.-T., & Mueller, E. 1996, *ApJL*, 473, L111  
 Kippenhahn, R., & Weigert, A. 1990, *Stellar Structure and Evolution*  
 Krause, F., & Raedler, K.-H. 1980, Oxford  
 Lattimer, J. M., & Swesty, D. F. 1991, *NuPhA*, 535, 331  
 Ledoux, P. 1947, *ApJ*, 105, 305  
 Masada, Y., Sano, T., & Shibata, K. 2007, *ApJ*, 655, 447  
 Masada, Y. 2011, *MNRAS*, 411, L26  
 Masada, Y., Takiwaki, T., Kotake, K., et al. 2012, *ApJ*, 759, 110  
 Masada, Y., & Sano, T. 2014, *ApJL*, 794, L6  
 Masada, Y., Takiwaki, T., & Kotake, K. 2015, *ApJL*, 798, L2  
 Miesch, M. S. 2005, *Living Reviews in Solar Physics*, 2, 1

- Moffatt, H. K. 1978, Cambridge Monographs on Mechanics and Applied Mathematics
- Mösta, P., Ott, C. D., Radice, D., et al. 2015, *Nature*, 528, 376
- Nagakura, H., Burrows, A., Radice, D., et al. 2019, arXiv:1912.07615
- Nordlund, Å., Galsgaard, K., & Stein, R. F. 1994, NATO Advanced Science Institutes (ASI) Series C, 471
- Ott, C. D., Burrows, A., Thompson, T. A., et al. 2006, *ApJS*, 164, 130
- Parker, E. N. 1955, *ApJ*, 122, 293
- Pedlosky, J. 1982, *Geophysical Fluid Dynamics* (Springer)
- Racine, É., Charbonneau, P., Ghizaru, M., et al. 2011, *ApJ*, 735, 46
- Raynaud R., Guilet J., Janka T. and Gastine, T, *Science Advances*, in press, hal-02428428
- Ruderman, M. 1972, *ARA&A*, 10, 427
- Ruderman, M. A., & Sutherland, P. G. 1973, *Nature Physical Science*, 246, 93
- Sano, T., Inutsuka, S., & Miyama, S. M. 1999, *Numerical Astrophysics*, 383
- Schekochihin, A. A., Cowley, S. C., Taylor, S. F., et al. 2004, *ApJ*, 612, 276
- Spruit, H. C. 2008, 40 Years of Pulsars: Millisecond Pulsars, Magnetars and More, 391
- Tassoul, J.-L. 2000, *Stellar rotation / Jean-Louis Tassoul*. Cambridge University Press
- Thompson, C., & Duncan, R. C. 1993, *ApJ*, 408, 194
- Yadav, R. K., Christensen, U. R., Wolk, S. J., et al. 2016, *ApJL*, 833, L28